Metachronal swimming of mantis shrimp: kinematics and interpleopod vortex interactions

Kuvvat Garayev, David W. Murphy

Department of Mechanical Engineering, University of South Florida, Tampa, FL 33620

Corresponding author contact:
David Murphy
Assistant Professor
Department of Mechanical Engineering
University of South Florida
4202 E. Fowler Ave
Tampa, FL 33620
E-mail: davidmurphy@usf.edu

Tel: 205-746-9135

Article word count: 5976

Abstract

Mantis shrimp swim via metachronal rowing, a pattern in which the pleopods (swimming limbs) stroke sequentially, starting with the last pair and followed by anterior neighbors. A similar swimming pattern is used at various sizes, Reynolds numbers, and advance ratios by diverse organisms including ciliates, ctenophores, copepods, krill, and lobsters. Understanding this type of locomotion is important because it is widespread and may inspire the design of underwater vehicles where efficiency, robustness, and maneuverability are desired. However, detailed measurements of the flow around free-swimming, metachronally rowing organisms are scarce, especially for organisms swimming in a high Reynolds number regime ($Re \ge 10^4$). In this study, we present time-resolved, planar PIV measurements of a swimming peacock mantis shrimp (Odontodactylus scyllarus). Simultaneous kinematics measurements of the animal, which had body and pleopod lengths of 114 mm and 20 mm, respectively, reveal mean swimming speeds of 0.2-1.9 m s⁻¹ and pleopod beat frequencies of 3.6-13 Hz, corresponding to advance ratios of 0.75-1.84 and bodybased Reynolds numbers of 23,000-217,000. Further, the animal's stroke is not purely metachronal, with a long phase lag between initiation of the first and fifth pleopod power strokes. Flow measurements in the sagittal plane show that each stroking pleopod pair creates a posteriorly moving tip vortex which evades destruction by the recovery strokes of other pleopod pairs. The vortex created by the anteriormost pleopod pair is the strongest and, owing to the animal's high advance ratio, is intercepted by the power stroke of the posteriormost pleopod pair. The vortex strength increases as a result of this interaction, which may increase swimming speed or efficiency. A relationship for vortex interception by the posterior pleopod is proposed that relates the phase lag between the interacting pleopods to the beat frequency, distance between those pleopods, and speed of the vortex relative to the animal. We describe this interaction with a novel parameter called the interpleopod vortex phase matching Strouhal number St_{IVPM} which is equal to the phase lag between interacting pleopods. This new nondimensional parameter may be useful in predicting the conditions where a constructive interaction may occur in other species or in physical models. Finally, we relate the advance ratio to the Reynolds number ratio, the ratio between the body-based Reynolds number and the pleopod-based Reynolds number. The importance of these parameters in promoting the interpleopod vortex interactions identified here, in dynamically scaled experiments, and in wake signatures behind schooling metachronal swimmers is discussed.

Introduction

Metachronal swimming is a type of locomotion used by ciliated and multi-limbed animals in which appendages stroke sequentially by allowing a time delay between adjacent appendages. Animals across a broad range of sizes, taxonomic classifications, and Reynolds numbers use this type of locomotion. Examples include ciliates (Blake & Sleigh, 1974), copepods (Jiang & Kiørboe, 2011), ctenophores (Sleigh, 1968), krill (Kils, 1981), mantis shrimp (Campos et al., 2012), and lobsters (Davis, 1968; Lim & DeMont, 2009). Crustaceans such as krill and mantis shrimp use adlocomotory metachronal swimming in which the posterior pleopod pair initiates the power stroke followed by anterior neighbors (Sleigh & Barlow, 1980). Metachronal swimming is used to accomplish a wide variety of swimming behaviors including long distance travel and high thrust escapes. For example, Antarctic krill may travel 12 km day-1 on average for several days (Kanda et al., 1982), copepods may accelerate up to 50 m s⁻² during their escape jumps (Jiang & Kiørboe, 2011; Murphy et al., 2012), and mantis shrimp may swim at speeds up to 40 body lengths s⁻¹ (BL s⁻¹) during escape responses (Campos et al., 2012). Further, metachronal swimming occurs across a wide range of sizes (paramecia; Niedermayer et al., 2008, to lobsters; Lim & DeMont, 2009), swimming speeds (up to 1.3 m s⁻¹; Campos et al., 2012), advance ratios (0.1-1.7; Murphy et al., 2011, Catton et al., 2011), and Reynolds numbers (O(10⁻⁴-10⁵); Niedermayer et al., 2008, Campos et al., 2012). Here, the advance ratio I is defined as the ratio of the animal mean swimming speed \bar{V} to the mean appendage tip speed \overline{U} ($I = \overline{V}/\overline{U}$). Animals with multiple pairs of appendages such as euphausiids and mantis shrimp tend to have "high" advance ratios (i.e. J~1 or J>1), meaning that their mean swimming speed is greater than their mean appendage tip speed (Murphy et al., 2011; Campos et al., 2012). In contrast, swimming animals

with only a single pair of appendages tend to have much lower advance ratios (J~0.1-0.6; Walker, 2002). The body-based Reynolds number Re_b is a dimensionless number representing the ratio of inertial to viscous forces ($Re_b = \bar{V}L/\nu$), where L is the body length and ν is the kinematic viscosity. The capabilities of metachronal swimmers have motivated researchers to try to understand the flow physics underlying metachronal rowing at different scales and apply it to novel device design (Dudek et al., 2007; Larson et al., 2014; Ford & Santhanakrishnan, 2020; Simha et al., 2020).

Previous researchers have investigated metachronal swimming using measurements of live organisms (Catton et al., 2011; Murphy et al., 2011; Campos et al., 2012; Murphy et al., 2013), robotic models (Ford et al, 2019; Ford & Santhanakrishnan, 2020; Hayashi & Takagi, 2020), computational fluid dynamics (CFD) simulations (Zhang et al., 2014; Granzier-Nakajima et al., 2020), and analytical models (Alben et al., 2010; Takagi, 2015). Many studies on live organisms have largely focused on acquiring measurements of appendage kinematics (Stamhuis & Videler, 1998a; Lenz et al., 2004; Murphy et al., 2011; Campos et al., 2012). Other research has focused on flow measurements around tethered animals (Yen et al., 2003; Patria & Wiese, 2004) or on stationary animals on the substratum (Stamhuis & Videler, 1998b; Lim & DeMont, 2009; Sensenig et al., 2010). While informative, tethering affects the flow field (Catton et al., 2007), thereby preventing a true understanding of the flow around the appendages. Only a few studies to date have looked at the flow around the appendages of freely swimming metachronal swimmers at relatively high Reynolds numbers ($Re \ge 10^4$; Daniel et al., 1992). For example, Catton et al. (2011) measured the flow around freely swimming Antarctic krill (Euphausia superba) and Pacific krill (Euphausia pacifica), but these measurements lacked the spatial and temporal resolution to determine flow structure development around the pleopods. Murphy et al. (2013) measured the flow around a hovering Antarctic krill using high speed tomographic PIV and found lift-generating tip vortices on the pleopod exopodites and oscillatory jet flow in the wake. Similarly, Colin et al. (2020) measured the flow around the appendages of ctenophores, tomopterid worms, and larval decapods swimming at Re<100 and found that negative pressures on the leeward sides of the stroking appendages contributed substantially to thrust. Further understanding flow

around metachronally stroking appendages might reveal additional mechanisms responsible for efficient or high-thrust locomotion.

Other researchers have used dynamically scaled robotic models to investigate the fluid dynamics and force generation of metachronal rowing. For example, Ford et al. (2019) and Ford and Santhanakrishnan (2020) used a dynamically scaled hovering (HOV) and fast forward swimming (FFW) "krillbot" to investigate the effects of varying Re and phase lag on swimming performance and found that the largest speeds and thrusts occurred with phase lag range of 15-25 %, coincident with those observed in E. superba in its FFW gait (Ford et al., 2019; Ford & Santhanakrishnan, 2020). Similarly, Hayashi and Takagi (2020) used a dynamically scaled robot with two legs to model metachronal rowing by microscopic crustaceans at Reynolds numbers less than unity, and showed that both non-zero phase difference and distinct mid-angles between the legs were necessary for the net movement of the model. However, robotic models to date have been limited to low Reynolds numbers (Hayashi & Takagi, 2020) or to low advance ratios (Ford & Santhanakrishnan, 2020; Hayashi & Takagi, 2020) compared to their live counterparts (Lenz et al., 2015; Murphy et al., 2011), a trend likely due to differences in appendage characteristics (e.g. morphology, changes in appendage shape throughout the stroke, rigidity, absence of fringe of setae). Finally, others have used CFD to investigate the efficiency of a stationary, metachronally paddling model with multiple rigid legs assuming 2D flow in the low to intermediate Re range (Zhang et al., 2014; Granzier-Nakajima et al., 2020). For example, Zhang et al. (2014) found that efficiency peaked at a phase lag of 12.5 % for a 4-legged model, and Granzier-Nakajima et al. (2020) found that a phase lag of 20-25 % yielded the highest average flux independent of stroke frequency. However, no simulations of a self-propelled metachronal swimmer have yet been conducted, thus precluding a detailed analysis of flow around the appendages.

Owing to a lack of simultaneous flow and kinematics measurements around free-swimming organisms, metachronal rowing at high speeds and high Reynolds numbers is not well understood. Further, many of the animals which use metachronal rowing at high speeds also have high advance ratios. At such high relative speeds, flows generated by anterior appendages may possibly interact constructively with those

produced by posterior appendages. Further, the lower influence of viscosity at these high Reynolds number may allow flow features (e.g. vortices) produced by one appendage to last long enough to synergistically interact with the stroke of another appendage for energy savings or enhanced thrust. Because of their availability and large size, mantis shrimp offer an excellent opportunity to understand the hydrodynamics of high speed metachronal rowing and to investigate the existence of synergistic flow interactions among appendages. The goal of this study is to use mantis shrimp to understand the hydrodynamics of high speed metachronal rowing and to investigate the existence of synergistic flow interactions among appendages at high J and intermediate to high Re.

Materials and Methods

Experimental Setup

An adult female peacock mantis shrimp (KP Aquatics LLC) was held in a 20 gallon, optically clear acrylic aquarium (61×33×41 cm³) filled with artificial seawater (Instant Ocean; salinity of 34 ppt; temperature of 26°±2° C). Water filtration and oxygenation were turned off only during experiments, and a diel light cycle was maintained. The aquarium contained ceramic biomedia cubes, live rock rubble, and a horizontal burrow (e.g. PVC pipe). The animal was fed weekly with mussels, clams, and shrimp and died after experiments were completed. Body length, posteriormost pleopod length, average pleopod length, and average spacing between pleopods were measured as 114 mm, 20 mm, 22 mm (± 1 mm, standard deviation), and 7.5 mm (± 0.5 mm, standard deviation), respectively.

Figure 1 shows the particle image velocimetry (PIV) system. The aquarium sat on a clear acrylic sheet (thickness of 12.7 mm) that was mounted on an extruded aluminum frame (80/20 Inc.) so that laser light could be directed upwards from below the aquarium in order to illuminate pleopod-generated flow. The sides and back of the aquarium were covered to reduce visual distractions to the animal and for laser safety.

The near-infrared laser (808 nm wavelength; 300W Firefly, Oxford Lasers, Inc, MA, USA) was mounted on a vertical optical rail enclosed within the frame by black HDPE panels. The light sheet emitted from the laser was further spread using a plano-concave cylindrical lens (Focal length = -19 mm, LK1037L1-B, Thorlabs Inc.). A high speed camera (Phantom VEO 640S, Vision Research, Inc, NL, USA) with 2560×1600 monochrome resolution equipped with a 50 mm lens (Nikon) was mounted on a horizontal optical rail (XT95SP-500, Thorlabs Inc., NJ, USA) on the aluminum frame such that its height and its distance from the aquarium (set at 50 cm) could be adjusted. The camera and laser were synchronized with a programmable timing unit (PTU X, LaVision, GmbH, Göttingen, Germany). Laser pulse duration was 100 μs in all tests. The experimental setup was mounted on an optical table. Seeding particles (20 μm polyamide, 1108948, LaVision) were mixed into the tank before an experiment and were subsequently filtered out. The PIV system was calibrated by imaging a ruler inserted into the tank that was coplanar with the laser sheet.

Mantis shrimp eyes can detect wavelengths of light ranging from UV to near-infrared, though this sensitivity differs among species (von Vaupel Klein, 2014). A study by Cowles et al. (2006) suggested no response to near-infrared light in *Hemisquilla californiensis*. However, the mantis shrimp in our study could detect the laser and avoided it during initial experiments. In order to encourage the animal to swim in the light sheet, parallel sheets of plastic separated by 45 mm - about twice the width of the mantis shrimp's abdomen (25.5 mm) - were placed on either side of the laser sheet in the tank. The front sheet (closer to the camera) was optically clear acrylic, and the back sheet was black HDPE to block reflections. It was judged that these walls would likely not affect the flow generated close to the animal's pleopods, and they were necessary to acquire data of the animal swimming in the correct orientation within the light sheet. At the beginning of each experiment, the animal was encouraged to swim by tapping on the side of the aquarium or by threatening it with a plastic rod inserted into the water near the aquarium wall, thereby encouraging the animal to swim into the quiescent water in the field of view. The recording was started in synchrony with the threat. With this setup, two flow measurement sequences in the animal's sagittal plane (Video

Sequences 1 and 2) and one sequence in the animal's near-frontal plane (Video Sequence 3) were acquired. In one additional case without the sheets present, the animal swam headfirst through the light sheet, allowing flow measurements in its transverse plane (Video Sequence 4). Table 1 gives an overview of the 4 data sets analyzed here, including camera frame rate, field of view, spatial resolution, video sequence length, and number of complete power and recovery strokes.

Processing and Analysis

In Video Sequences 1-2, pleopod kinematics were manually extracted at a temporal resolution of 100 Hz using ImageJ (National Institutes of Health, USA). As shown in Figure 2, three points on each pleopod were tracked. The first point was the endopodite tip (red in Figure 2), and the second point was the joint between the protopodite and the endo/exopodite (green in Figure 2). The proximalmost protopodite point visible in the lateral view was tracked as the third point (blue in Figure 2) because the protopodite's base was obscured by the abdominal segment. These points will be referred to as the base (blue), joint (green), and tip (red) points. A distinct spot on the carapace also was tracked for speed measurement using DLTdv7 (Hedrick, 2008). Figure 2 also shows the stroke angles α and β . Here α is defined as the angle formed between the protopodite and the base points of that protopodite and its anterior neighbor. For the anteriormost pleopod, the posterior neighbor base point is used for calculating α . Angle β is the angle between the protopodite and endo/exopodite. Animal swimming speed V was calculated by applying a central differencing scheme to tracked carapace points with a temporal resolution of 0.05 s, and normalized swimming speed was defined as $V_n = V/L$. For Video Sequences 1-3, the beat frequency of each pleopod was calculated as the reciprocal of the time between defined pleopod positions, and the mean pleopod beat frequency f was calculated as the average of these five frequencies. In Video Sequence 4, since not all pleopods were visible, the beat frequency was estimated based on the power stroke duration of P5.

As shown in Table 1, additional parameters, including phase lags between sequentially beating pleopods, pleopod- and body-based Reynolds numbers, advance ratio, and Strouhal number also were calculated.

Phase lag Ψ is defined as the time between the start of power strokes of consecutively stroking pleopods normalized by stroke period. The pleopod-based Reynolds number, Re_p , is defined in a coordinate system moving with the animal as

$$Re_p = \frac{l\overline{U}}{v} = \frac{2\theta f l^2}{v}$$

where l is the pleopod length and θ is stroke amplitude. Here, the mean tip speed \overline{U} is calculated approximating pleopod motion as harmonic. The advance ratio J (Ellington, 1984), defined as the ratio of the animal mean forward speed to the mean appendage tip speed, is calculated as

$$J = \frac{\overline{V}}{2\theta f l}.$$

Finally, the Strouhal number St is defined as

$$St = \frac{f l_c}{\overline{V}}$$

where $l_c = 2lsin(\theta/2)$ is the excursion of the pleopod tip during the power stroke (Taylor, 2003; Murphy et al., 2013). Calculations of Re, J, and St are performed using the length and stroke amplitude of the fifth pleopod.

DaVis 8 software (LaVision GmbH, Göttingen, Germany) was used to calculate the time-resolved velocity fields through multi-pass cross-correlation of a time-series of consecutive frames utilizing a dynamic mask (i.e. the mantis shrimp silhouette) which was created in three steps. First, a white top-hat operation available in the ImageJ plugin (MorphoLibJ, Legland et al., 2016) was applied on raw images to remove the animal. Second, the resultant images were subtracted from the raw images to remove seeding particles from the raw images. Third, images from the second step were binarized and any residual dots were removed using Analyze Particles operation in ImageJ. Velocity vectors were calculated in interrogation areas of 48×48

pixels in the first pass and 32×32 pixels in the following three passes, with 50% overlap between adjacent interrogation areas. In post-processing, velocity vectors were removed if the peak ratio Q was less than 1.2.

Results

Kinematics

As shown in Table 1, the animal in Video Sequence 1 swam at $\bar{V}=0.20\pm0.03$ m s⁻¹ (mean \pm standard deviation), $\bar{V}_n=1.8\pm0.3$ BL s⁻¹, f=3.6 Hz, and J=0.75. The corresponding Re_p and Re_b were 5,000 and 23,000, respectively, and the St was 0.58. The animal in Video Sequence 2 swam faster, at $\bar{V}=0.39\pm0.04$ m s⁻¹, $\bar{V}_n=3.4\pm0.4$ BL s⁻¹, f=4.8 Hz, and J=1.02. The animal in Video Sequence 3 (from a near-frontal view) swam even faster, at $\bar{V}=0.57\pm0.04$ m s⁻¹, $\bar{V}_n=5.0\pm0.4$ BL s⁻¹, f=7.6 Hz, and an estimated J=0.94 (assuming a stroke amplitude of 114°). Finally, the animal in Video Sequence 4 (from a transverse view) swam at approximately $\bar{V}=1.9\pm0.2$ m s⁻¹, estimated by dividing the length of the animal by the time it was present in the laser sheet, and the corresponding \bar{V}_n was 16.7 ± 1.8 BL s⁻¹. Owing to the animal's orientation in the laser sheet, the animal's beat frequency was thus estimated to be 13 Hz by measuring the power stroke duration of P5 and using the ratio of power stroke duration to recovery stroke duration found from Video Sequence 1 to calculate the entire stroke duration. This beat frequency is somewhat smaller than the beat frequency of 17 Hz observed by Campos et al. (2012) for escaping *Odontodactylus havanensis*, a trend that is expected based on the larger animal examined here. Again assuming a stroke amplitude of 114° , the mantis shrimp in Video Sequence 4 swam with an estimated J=1.84.

Figures 3A and 3B show the time history of the pleopod angles α and β , respectively, for all five pleopods over approximately two strokes measured from Video Sequence 1. Values of α increase as the animal performs its power stroke and decrease during the recovery stroke. Minimum values of α are similar for all pleopods and range from 27° to 40°. In contrast, maximum values of α decrease from posterior to anterior,

with P5 reaching a maximum α of 143° and P1 reaching a maximum α of 126°. The amplitude of P5 was approximately 106°. Values of β are at their maxima during each pleopod's power stroke and at their minima during each pleopod's recovery stroke. Maximum and minimum values of β at this swimming speed are approximately 190° and 103°, respectively. Finally, Table 1 shows that Ψ is approximately 15% for the adjacent pleopod pairings (e.g. P5-P4, P4-P3, P3-P2, and P2-P1) but is approximately 40% for the anterior-posterior pleopod pairing (e.g. P1-P5), thus indicating that the mantis shrimp stroke is not purely metachronal.

Figure 3C shows the time history of V in Video Sequence 1. The colored bars represent the beginning and end of each pleopod's power stroke and correspond to the kinematics presented in Figure 3A-B. In Fig. 3C, the animal swims at $\overline{V} = 0.20 \,\mathrm{m \ s^{-1}}$, accelerates and decelerates in response to its power and recovery strokes, and accelerates slightly overall. Since V is periodic and oscillates around a mean, the periodic amplitude was defined as the difference between the mean and maximum swimming speeds and was found to be $0.02 \,\mathrm{m \ s^{-1}}$. The increases in speed correspond to the onset of the power stroke of P4. However, the animal has reached its peak speed during the power stroke of P2 and subsequently decelerates during the power stroke of P1. The available kinematics data for Video Sequences 2-4 are presented in the Supplementary Material.

Flow Fields

Figure 4 shows a series of measured flow fields from Video Sequence 1. In Fig. 4A (at t = 0.315 s), the mantis shrimp is swimming at V = 0.24 m s⁻¹, has just completed the power stroke of P3, and is midway through the power stroke of P2. The vortex created by the power stroke of P3 is highlighted in blue (corresponding to the color indicating P3 in Figure 3), and the vortex being formed by the power stroke of P2 also can be seen (not highlighted). A vortex previously created by the stroke of P4 also can be seen beneath the telson. In Fig. 4B (at t = 0.350 s), the mantis shrimp has moved forward several millimeters and has completed the power stroke of P2, leading to the full formation of a tip vortex (highlighted in green). The vortex previously generated by P3 is not apparent in this frame but, in the video, appears to

have been advected such that it lies at the tip of P5. In Fig. 4C (at $t = 0.410 \, s$), the mantis shrimp is swimming at $V = 0.20 \, \text{m s}^{-1}$ and has completed the power stroke of P1, leading to the formation of a vortex highlighted in red. The vortex generated by P1 is stronger than those previously generated by the other pleopods, which have been advected downstream and have dissipated somewhat by this time. In Fig. 4D (at $t = 0.440 \, s$), the vortex generated by P1 has been advected backwards even as the animal has moved forward. Further, the vortex has not been weakened by the nearly simultaneous recovery of the five pleopod pairs. In Fig. 4E (at $t = 0.5 \, s$), the vortex generated by P1 is intercepted and strengthened by P5, which is now midway through its power stroke. Specifically, the vortex circulation Γ , calculated in TecPlot 360 (Tecplot, Bellevue, WA) by integrating vorticity over the area with vorticity threshold above $5 \, s^{-1}$, is approximately 2409 mm² s⁻¹ at $t = 0.410 \, s$ (Fig. 4C), slightly decreases to 1984 mm² s⁻¹ at $t = 0.440 \, s$ (Fig. 4D), and subsequently increases to 3472 mm² s⁻¹ at $t = 0.500 \, s$ (Fig. 4E) owing to the action of P5. This vortex interception mechanism is illustrated in Figure 5 and will be discussed in detail later.

The now-visible wake behind the mantis shrimp is seen to comprise a backwards jet with flow speeds up to 0.14 m s^{-1} . Flow appears to be entrained down into this jet from above the animal but not from below. This may be due to the fact that the animal was slightly descending as it was swimming forward. In Fig. 4F (at t = 0.530 s), the vortex generated by P1 and strengthened by P5, now highlighted in cyan, is located beneath the base of the telson. Pleopod pair P4 is midway through its power stroke and its vortex is highlighted in magenta. In Fig. 4G (at t = 0.565 s), the vortex previously generated by P5 is shown in cyan. By this time, P4 has completed its power stroke, and its vortex is highlighted in magenta. In Fig. 4H (at t = 0.760 s), the animal has moved substantially such that only its telson is visible in the cropped field of view. The wake of the animal resembles a reverse von Karman vortex street with counter-rotating vortices creating a jet of flow directed backwards. Vortices created by the pleopods since t = 0.410 s (Fig. 4C) are contained in the dashed rectangle in yellow. The flow reaches speeds of up to 0.18 m s^{-1} in the rectangle containing this jet. Measured flow fields for Video Sequences 2-4 are presented in the Supplementary Material.

Discussion

Previous experimental studies of the flow induced by metachronal rowing at Reynolds numbers of 10^2 - 10^3 have focused on tethered (i.e., stationary) (Yen at al., 2003), hovering (Murphy et al., 2013), or slowly swimming animals (Catton et al., 2011), stationary robotic models (Ford et al., 2019), or robots moving at low advance ratios (Ford et al., 2020). Further, computational studies have only investigated metachronal stroking by non-translating (i.e., stationary) appendages (Zhang et al., 2014; Granzier-Nakajima et al., 2020). Theoretical studies of simplified appendage models stroking in a metachronal fashion are also available in the literature (Takagi, 2015; Hayashi & Takagi, 2020). Questions about how flows induced by individual appendages may vary with swimming speed or how these flows may synergistically interact to enhance locomotive performance have thus remained unanswered. For the first time, this study provides time-resolved flow measurements of a metachronal rower swimming at high advance ratios (J~1) as well as measurements of the appendage kinematics producing those flows. These kinematics and flow field measurements give new insight into how flow interactions among pleopods may be important in metachronal swimming at high advance ratios.

Kinematics

This study reveals important aspects of mantis shrimp swimming kinematics and of metachronal swimming kinematics in general. The pleopod kinematics measured here show that the mantis shrimp stroke is not purely metachronal, with non-uniform values of Ψ for different consecutively stroking appendage pairs. The long P1-P5 phase lag between the initiation of the most anterior pleopod's power stroke and the beginning of the next stroke by the most posterior pleopod pair (Ψ =~40%) lies in contrast to the almost purely metachronal stroking of fast forward swimming Antarctic krill (Murphy et al., 2011), where Ψ equals approximately 20% for all appendage pairings. For the mantis shrimp, the long P1-P5 phase lag may be related to the faster (i.e. shorter duration) power strokes as compared to slower recovery strokes, which

may be an adaptation for generating high levels of thrust for escape swimming. Such variations to a pure metachronal stroke pattern, which are not well understood, are widespread (Lim & DeMont, 2009) and may include pauses to allow for synchronous recovery (Alexander, 1988; Boudrias, 2002; van Duren & Videler, 2003). It should also be noted that, in contrast to the unsupported claim by Campos et al. (2012) for *O. havanensis*, the mantis shrimp recovery stroke is not truly synchronous, though the close pleopod spacing and anteriorly decreasing median stroke angle make it appear so.

Further comparing *O. scyllarus* with Antarctic krill, the stroke amplitudes of both species are similar and generally decrease from posterior to anterior. However, the median angle of the pleopod stroke, defined here as $\bar{\alpha} = (\frac{\alpha_{min} + \alpha_{max}}{2})$ (Hayashi & Takagi, 2020) differs between these two species. Values of $\bar{\alpha}$ were 91-95° and 67° for the mantis shrimp and FFW swimming Antarctic krill, respectively (Murphy et al., 2011). The greater values of $\bar{\alpha}$ for the mantis shrimp indicate that the pleopod-generated flow is more posteriorly directed, which may be useful for generating thrust and high swimming speeds. In contrast, the lower $\bar{\alpha}$ values for Antarctic krill may indicate that flow is directed downwards to a greater extent, a lift-generating adaptation useful in a nektonic lifestyle. Finally, the animal swimming speeds and beat frequencies measured here closely correspond with those of *O. havanensis* (Campos et al., 2012) for individuals smaller than that examined here. For the 114 mm *O. scyllarus* examined here, swimming speeds ranged from 1.8 to 16.7 BL s⁻¹ while beat frequencies ranged from 3.6 to 13 Hz. On the other hand, escaping *O. havanensis* with body lengths 35-64 mm swam at speeds 21-40 BL s⁻¹ with mean beat frequency of 17 Hz (Campos et al., 2012).

Finally, it is important to note that the inner pleopod pairs (P2-P4) fold during the recovery stroke to values of β that are small enough to allow the undisturbed backwards translation of the jet created by P1 (Fig. 4D). This configuration eliminates the adverse interference between the pleopods and the P1-created backward flow and also allows the vortex interaction between P1 and P5. This suggests that active control of distal pleopod parts (endo/exopodites) is an important design parameter which could be incorporated into future

physical models. In addition, it is interesting to note that the angle between the protopodite and the distal pleopod segments appears to extend past 180° during the power stroke (e.g. Fig. 3B), thereby forming an anteriorly concave appendage surface. A similar appendage configuration has been seen in other metachronally stroking organisms and linked to low pressure, thrust-generating regions (Colin et al., 2020) and may also serve that purpose here. However, it seems unlikely that this configuration arises from bending of the distal appendage owing to its greater rigidity relative to the flexible appendages of those organisms studied by Colin et al. (2020).

Hydrodynamics

A significant flow phenomenon observed in the PIV measurements (e.g. Fig. 4, Supplementary Fig. 2) is that the vortex produced by pleopod pair 1 advects backwards while posterior pleopods recover such that pleopod pair 5 strokes into the P1 vortex and strengthens it. Specifically, the measured flow fields show that the newly produced P1 vortex is advected backwards at speeds of approximately 0.06 m s⁻¹ at the same time that the animal continues to translate forward at higher speeds ranging from 0.17 m s⁻¹ to 0.24 m s⁻¹ (Video Sequence 1). As a result of this difference in relative speeds, the P1 vortex is positioned directly beneath pleopod pair p5 during its power stroke. The mantis shrimp may exploit this vortex as it strokes its posteriormost pleopod pair into the P1 vortex (e.g. Fig. 4, Supplementary Fig. 2). This interaction may save the mantis shrimp energy by allowing the pleopod to stroke into flow that is already moving to the posterior of the animal. Indeed, the animal attains peak swimming speeds just after this interaction (e.g. Fig. 3C, Supplementary Fig. 1B-C) and produces its maximum jet velocity due to this interaction (e.g. Supplementary Fig. 5).

Numerous other studies have found energy savings through the exploitation of vortices shed either by a stationary object (Liao et al., 2003), a nearby conspecific (Li at al., 2020), or another part of that animal's body (Drucker & Lauder, 2001), and the current flow measurements provide the first evidence that a similar energy saving mechanism is present in the pleopods of metachronally swimming organisms. For example,

Drucker and Lauder (2001) proposed that swimming bluegill sunfish save energy by stroking their caudal fin into the vortex shed by the dorsal fin, thereby enhancing its circulation. On a larger scale, exploitation of vortices to save energy in bird flocks is a well-known phenomenon. For instance, Portugal et al. (2014) have shown that the follower birds in a V formation arrange the phase of their wingstrokes such that they benefit from the previously shed upwash generated by an anterior neighbor. Similarly, Li et al. (2020) investigated leader-follower pairs of live fish and robotic fish and found that the follower fish saved energy at certain spatiotemporally dependent phases relative to the leader fish owing to the phase-dependent vortex flow generated by the leader's caudal fin, a phenomenon called vortex phase matching (VPM). These authors derived the following analytical formula to describe this spatiotemporal dependence:

$$\Phi = \Phi_o + \frac{2\pi f}{u}D$$

Here Φ is the phase difference between undulations of the follower and leader fishes; Φ_o is the phase difference between undulation of the follower fish and the vortex-induced flow with which it interacts; f is the tailbeat frequency; u is swimming speed; and D is the front-back distance between the leader and follower. The follower fish saves energy when it adopts a phase difference Φ within a certain range of values (Li et al., 2020).

We propose a similar relationship for the constructive interaction between a posterior appendage and a vortex created by an anterior appendage in an adlocomotory metachronal swimmer:

$$\Psi_{a-p} \approx f \frac{B}{u}$$

Here, Ψ_{a-p} is the phase lag between the anterior and posterior appendages (subscript a stands for the anterior appendage that releases the vortex; subscript p stands for the posterior appendage that intercepts the released vortex), f is the pleopod beat frequency, u is the vortex speed relative to the animal speed (i.e. u = v + V, where v is the vortex speed in the laboratory reference frame), and B is the distance between

base articulations of interacting appendages. As illustrated in Figure 5, this expression states that the constructive vortex interaction will occur when the phase lag Ψ_{a-p} approximately equals the portion of the stroke it takes for the generated vortex to travel to the posterior appendage. For example, in the mantis shrimp, P5 has to stroke with a phase lag of Ψ_{P1-P5} during the time interval B/u in order to interact with the vortex released by P1. For Video Sequence 1, the P1-P5 phase lag as measured from the pleopod kinematics is $\Psi_{P1-P5} = 0.42$ (Table 1). This matches well with the calculated value of $f \frac{B}{u} = 0.43$, where the time interval $\frac{B}{u}$ was measured as 0.12 s and f = 3.6 Hz. Similarly, for Video Sequence 2, $\Psi_{P1-P5} = 0.37$ and $f \frac{B}{u} = 0.36$. We further note that the quantity $f \frac{B}{u}$, which relates a frequency, length, and speed, is a type of nondimensional Strouhal number which we call the interpleopod vortex phase matching Strouhal number Stiypm, defined as

$$St_{IVPM} = \frac{fB}{u}$$

where $St_{IVPM} \approx \Psi_{a-p}$. For the mantis shrimp steadily swimming at $J \approx 1$, we find from Table 1 that $\Psi_{P1-P5} \approx St_{IVPM} \approx 0.4$. This nondimensional parameter, which considers both the wake speed and animal speed, may be useful in predicting the conditions where constructive vortex interaction may occur in other metachronally swimming species. In physical models, one can tune the parameters in the above equation to benefit from interpleopod vortex phase matching. However, it is important to note that this interaction may not always occur between the anteriormost and posteriormost appendages. For example, in the nearly fast forward swimming Antarctic krill (swimming speed = 1.7 BL s⁻¹) studied by Catton et al. (2011), the flow generated by the P1 pleopod appears to interact with the P4 pleopod. In this instance, f = 3 Hz, $B \approx 1.05$ cm, and $u \approx 9$ cm s⁻¹, resulting in a $St_{IVPM} \approx 0.35$, which is close to the P1-P4 phase lag of fast forward swimming Antarctic krill (0.38) previously measured by Murphy et al. (2011).

Interpleopod vortex phase matching (IVPM) as a constructive interaction strategy may only occur under certain circumstances. For example, IVPM occurred when the mantis shrimp swam at a constant cycle-

averaged speed in a straight line. Later frames of Video Sequence 2 (e.g. Supplementary Figure 3) show the animal pitching up such that the animal's last pleopod pair misses the P1 vortex. Further, IVPM may only be available to animals swimming at Re high enough for vortices to form and be advected a given distance without dissipating owing to the effects of viscosity. For example, significant appendage tip vortices do not seem to form for most metachronal swimmers at $Re_p < \sim 100$ (Colin et al., 2020). In contrast, tip vortices did form at Re_p range of 5,000-29,000 for the mantis shrimp pleopods and 310-360 for hovering Antarctic krill (Murphy et al., 2013). Finally, IVPM may not occur at all swimming speeds or advance ratios. For example, an animal hovering at a low advance ratio may change its body angle, median stroke angle, and P1-P5 phase lag, thereby limiting the time available for the P1 vortex to travel to more posterior appendages or directing vortices away from posterior appendages (Murphy et al., 2011; Ford & Santhanakrishnan, 2020; Hayashi & Takagi, 2020).

In general, the flow that each pleopod will both experience and generate will naturally depend on the speed at which the animal is swimming, and the relation between the animal speed and the pleopod speed may determine the possibility of constructive vortex interactions. This relationship can be encapsulated by considering the ratio of the body Reynolds number to the pleopod Reynolds number, which we name the Reynolds number ratio and define here as

$$R = \frac{Re_b}{Re_p} = J\frac{L}{l}$$

For a given body geometry (defined by L and l), IVPM may only be available at certain values of J. Dynamically scaled experiments must necessarily match J in order to reproduce accurate flows around metachronally stroking appendages in dynamically scaled models. The krillbot, for example, closely matched J for a hovering krill but was too low for a krill performing FFW swimming (Ford & Santhanakrishnan, 2020). Further, dynamically scaled experiments on metachronally stroking paddles that are both translating and rotating in such a way that realistic J values are preserved would be useful in

understanding the flows and forces on these paddles and the potential for IVPM to enhance system performance. Finally, the impact of R on the wake signature behind metachronally swimming organisms ought to be investigated as this may play a role in hydrodynamic signaling among schooling conspecifics such as Antarctic krill (Murphy et al., 2019). For example, slowly swimming krill (i.e. low R) seem to generate a fairly coherent jet (Catton et al., 2011, Murphy et al., 2013), but a fast swimming krill (i.e. high R) may generate a much more spatially patchy or temporally oscillatory wake signature (e.g. Supplementary Fig. 5), with unknown implications for signaling.

Conclusions

Using planar, time-resolved PIV, we measured the pleopod kinematics and flow fields generated by the metachronal propulsion of a peacock mantis shrimp swimming at high advance ratios and Reynolds numbers. The animal's stroke is not purely metachronal, with a long phase lag between initiation of the power strokes by the first and fifth pleopods. The flow measurements reveal a possible energy savings technique we call interpleopod vortex phase matching wherein the vortex generated by the anteriormost pleopod pair is intercepted and strengthened by the stroke of the posteriormost pleopod pair. These results highlight the importance of considering the advance ratio in dynamically scaled, metachronally swimming physical models, a relationship encapsulated in R, the ratio of the body-based Re_b and the pleopod-based Re_n .

Data availability

Data will be shared on reasonable request to the corresponding author.

Funding

Funding was provided by grants from the National Academies of Science Keck Futures Initiative (NAKFI) and the National Science Foundation (OPP 1840941).

Acknowledgments

We gratefully acknowledge Michael Celestin for assistance in setting up the saltwater aquarium.

References

Alben, S., Spears, K., Garth, S., Murphy, D., & Yen, J. (2010). Coordination of multiple appendages in drag-based swimming. *Journal of The Royal Society Interface*, 7(52), 1545-1557.

Alexander, D. E. (1988). Kinematics of swimming in two species of Idotea (Isopoda: Valvifera). *Journal of experimental biology*, 138(1), 37-49.

Blake, J. R., & Sleigh, M. A. (1974). Mechanics of ciliary locomotion. *Biological Reviews*, 49(1), 85-125.

Boudrias, M. A. (2002). Are pleopods just "more legs"? The functional morphology of swimming limbs in Eurythenes gryllus (Amphipoda). *Journal of Crustacean Biology*, 22(3), 581-594.

Campos, E. O., Vilhena, D., & Caldwell, R. L. (2012). Pleopod rowing is used to achieve high forward swimming speeds during the escape response of Odontodactylus havanensis (stomatopoda). *Journal of Crustacean Biology*, 32(2), 171-179.

Catton, K. B., Webster, D. R., Brown, J., & Yen, J. (2007). Quantitative analysis of tethered and free-swimming copepodid flow fields. Journal of Experimental Biology, 210(2), 299-310.

Catton, K. B., Webster, D. R., Kawaguchi, S., & Yen, J. (2011). The hydrodynamic wake of two species of krill: Implications for signaling among schooling krill. *J Exp Biol*, 214, 1845-1856.

Colin, S. P., Costello, J. H., Sutherland, K. R., Gemmell, B. J., Dabiri, J. O., & Du Clos, K. T. (2020). The role of suction thrust in the metachronal paddles of swimming invertebrates. Scientific reports, 10(1), 1-8.

Cowles, D. L., Van Dolson, J. R., Hainey, L. R., & Dick, D. M. (2006). The use of different eye regions in the mantis shrimp Hemisquilla californiensis Stephenson, 1967 (Crustacea: Stomatopoda) for detecting objects. *Journal of experimental marine biology and ecology*, 330(2), 528-534.

Daniel, T., Jordan, C., & Grunbaum, D. (1992). Hydromechanics of swimming. Advances in comparative and environmental physiology, 11, 17-49.

Davis, W. J. (1968). Quantitative analysis of swimmeret beating in the lobster. Journal of Experimental Biology, 48(3), 643-662.

Drucker, E. G., & Lauder, G. V. (2001). Locomotor function of the dorsal fin in teleost fishes: experimental analysis of wake forces in sunfish. *Journal of Experimental Biology*, 204(17), 2943-2958.

Dudek, G., Giguere, P., Prahacs, C., Saunderson, S., Sattar, J., Torres-Mendez, L. A., ... & Zacher, J. (2007). Aqua: An amphibious autonomous robot. *Computer*, 40(1), 46-53.

Ellington, C. P. (1984). The aerodynamics of hovering insect flight. III. Kinematics. *Philosophical Transactions of the Royal Society of London. B, Biological Sciences*, 305(1122), 41-78.

Ford, M. P., Lai, H. K., Samaee, M., & Santhanakrishnan, A. (2019). Hydrodynamics of metachronal paddling: effects of varying Reynolds number and phase lag. *Royal Society Open Science*, 6(10), 191387.

Ford, M. P., & Santhanakrishnan, A. (2020). On the role of phase lag in multi-appendage metachronal swimming of Euphausiids. *bioRxiv*.

Granzier-Nakajima, S., Guy, R. D., & Zhang-Molina, C. (2020). A Numerical Study of Metachronal Propulsion at Low to Intermediate Reynolds Numbers. *Fluids*, *5*(2), 86.

Hayashi, R., & Takagi, D. (2020). Metachronal swimming with rigid arms near boundaries. *Fluids*, *5*(1), 24.

Hedrick, T. L. (2008). Software techniques for two-and three-dimensional kinematic measurements of biological and biomimetic systems. *Bioinspiration & biomimetics*, 3(3), 034001.

Jiang, H., & Kiørboe, T. (2011). Propulsion efficiency and imposed flow fields of a copepod jump. Journal of Experimental Biology, 214(3), 476-486.

Kanda, K., Takagi, K., & Seki, Y. (1982). Movement of the larger swarms of Antarctic krill Euphausia superba population off Enderby Land during 1976-1977 season. *Journal of the Tokyo University of Fisheries (Japan)*.

Kils, U. (1981). Swimming behaviour, swimming performance and energy balance of Antarctic krill Euphausia superba. BIOMASS Sci. Ser., 3, 1-121.

Larson, M., Kiger, K. T., Abdelaziz, K., & Balaras, E. (2014). Effect of metachronal phasing on the pumping efficiency of oscillating plate arrays. Experiments in fluids, 55(5), 1741.

Legland, D., Arganda-Carreras, I., & Andrey, P. (2016). MorphoLibJ: integrated library and plugins for mathematical morphology with ImageJ. *Bioinformatics*, *32*(22), 3532-3534.

Lenz, P. H., Hower, A. E., & Hartline, D. K. (2004). Force production during pereiopod power strokes in Calanus finmarchicus. *Journal of Marine Systems*, 49(1-4), 133-144.

Lenz, P. H., Takagi, D., & Hartline, D. K. (2015). Choreographed swimming of copepod nauplii. Journal of The Royal Society Interface, 12(112), 20150776.

Li, L., Nagy, M., Graving, J. M., Bak-Coleman, J., Xie, G., & Couzin, I. D. (2020). Vortex phase matching as a strategy for schooling in robots and in fish. *Nature Communications*, 11(1), 1-9.

Liao, J. C., Beal, D. N., Lauder, G. V., & Triantafyllou, M. S. (2003). Fish exploiting vortices decrease muscle activity. *Science*, *302*(5650), 1566-1569.

Lim, J. L., & DeMont, M. E. (2009). Kinematics, hydrodynamics and force production of pleopods suggest jet-assisted walking in the American lobster (Homarus americanus). *Journal of Experimental Biology*, 212(17), 2731-2745.

Morris, M. J., Gust, G., & Torres, J. J. (1985). Propulsion efficiency and cost of transport for copepods: a hydromechanical model of crustacean swimming. *Marine Biology*, 86(3), 283-295.

Murphy, D. W., Olsen, D., Kanagawa, M., King, R., Kawaguchi, S., Osborn, J., ... & Yen, J. (2019). The three dimensional spatial structure of Antarctic krill schools in the laboratory. *Scientific reports*, 9(1), 1-12.

Murphy, D. W., Webster, D. R., Kawaguchi, S., King, R., & Yen, J. (2011). Metachronal swimming in Antarctic krill: Gait kinematics and system design. *Marine biology*, *158*(11), 2541-2554.

Murphy, D. W., Webster, D. R., & Yen, J. (2013). The hydrodynamics of hovering in Antarctic krill. *Limnology and Oceanography: Fluids and Environments*, *3*(1), 240-255.

Niedermayer, T., Eckhardt, B., & Lenz, P. (2008). Synchronization, phase locking, and metachronal wave formation in ciliary chains. *Chaos: An Interdisciplinary Journal of Nonlinear Science*, *18*(3), 037128.

Patria, M. P., & Wiese, K. (2004). Swimming in formation in krill (Euphausiacea), a hypothesis: dynamics of the flow field, properties of antennular sensor systems and a sensory–motor link. Journal of plankton research, 26(11), 1315-1325.

Portugal, S. J., Hubel, T. Y., Fritz, J., Heese, S., Trobe, D., Voelkl, B., ... & Usherwood, J. R. (2014). Upwash exploitation and downwash avoidance by flap phasing in ibis formation flight. Nature, 505(7483), 399-402.

Sensenig, A. T., Kiger, K. T., & Shultz, J. W. (2010). Hydrodynamic pumping by serial gill arrays in the mayfly nymph Centroptilum triangulifer. Journal of Experimental Biology, 213(19), 3319-3331.

Simha, A., Gkliva, R., Kotta, Ü., & Kruusmaa, M. (2020). A Flapped Paddle-Fin for Improving Underwater Propulsive Efficiency of Oscillatory Actuation. IEEE Robotics and Automation Letters, 5(2), 3176-3181.

Sleigh, M. A. (1968). Metachronal co-ordination of the comb plates of the ctenophore Pleurobrachia. Journal of Experimental Biology, 48(1), 111-125.

Sleigh, M. A., & Barlow, D. I. (1980). Metachronism and control of locomotion in animals with many propulsive structures. *Aspects of animal movement*, 49-67.

Stamhuis, E. J., & Videler, J. J. (1998). Burrow ventilation in the tube-dwelling shrimp Callianassa subterranea (Decapoda: thalassinidea). I. Morphology and motion of the pleopods, uropods and telson. Journal of experimental biology, 201(14), 2151-2158.

Stamhuis, E. J., & Videler, J. J. (1998). Burrow ventilation in the tube-dwelling shrimp callianassa subterranea (Decapoda: thalassinidea). II. The flow in the vicinity of the shrimp and the energetic advantages of a laminar non-pulsating ventilation current. Journal of Experimental Biology, 201(14), 2159-2170.

Takagi, D. (2015). Swimming with stiff legs at low Reynolds number. *Physical Review E*, 92(2), 023020.

Taylor, G. K., Nudds, R. L., & Thomas, A. L. (2003). Flying and swimming animals cruise at a Strouhal number tuned for high power efficiency. *Nature*, 425(6959), 707-711.

van Duren, L. A., & Videler, J. J. (2003). Escape from viscosity: the kinematics and hydrodynamics of copepod foraging and escape swimming. *Journal of Experimental Biology*, 206(2), 269-279.

von Vaupel Klein, J. C. (Ed.). (2014). Treatise on Zoology-Anatomy, Taxonomy, Biology. The Crustacea, Volume 4. Brill.

Walker, J. A. (2002). Functional morphology and virtual models: physical constraints on the design of oscillating wings, fins, legs, and feet at intermediate Reynolds numbers. *Integrative and Comparative Biology*, 42(2), 232-242.

Yen, J., Brown, J., & Webster, D. R. (2003). Analysis of the flow field of the krill, Euphausia pacifica. *Mar. Fresh. Behav. Physiol.*, *36*(4), 307-319.

Zhang, C., Guy, R. D., Mulloney, B., Zhang, Q., & Lewis, T. J. (2014). Neural mechanism of optimal limb coordination in crustacean swimming. *Proceedings of the National Academy of Sciences*, 111(38), 13840-13845.

Author notes

From the symposium "Metachronal Coordination of Multiple Appendages for Swimming and Pumping" presented at the annual meeting of the Society for Integrative and Comparative Biology, Virtual: 3

January – 28 February 2021.

Table 1. Values of experimental and kinematics parameters for the four Video Sequences analyzed in the current study.

Video Sequence	1	2	3	4
Measurement Plane	Sagittal	Sagittal	Near-Frontal	Transverse
Frequency (frames s ⁻¹)	200	1000	1000	200
Field of View (cm×cm)	31.3×19.6	27.7×17.3	30.7×19.2	25.9×16.2
Resolution (µm pixel ⁻¹)	122.3	108.0	112.0	101.2
Duration (s)	0.56	0.40	0.30	0.10
Number of Strokes	2	2	2	1
Mean Swimming Speed \pm SD, $\bar{V} \pm$ SD (m s ⁻¹)	0.20±0.03	0.39±0.04	0.57±0.04	1.9±0.2
Normalized Mean Swimming Speed, \overline{V}_n (BL s ⁻¹)	1.8±0.3	3.4±0.4	5.0±0.4	16.7±1.8
Beat Frequency, $f(s^{-1})$	3.6	4.8	7.6	13
Phase Lag (P5-P4), Ψ_{P5-P4} (%)	11	15	15	-
Phase Lag (P4-P3), Ψ_{P4-P3} (%)	10	11	13	_
Phase Lag (P3-P2), Ψ_{P3-P2} (%)	17	15	17	_
Phase Lag (P2-P1), Ψ_{P2-P1} (%)	20	21	14	_
Phase Lag (P1-P5), Ψ_{P1-P5} (%)	42	37	40	-
P5 Stroke Amplitude, <i>θ</i> (°)	106	114	_	_
Pleopod-based Reynolds Number, Re_p (10 ³)	5	8	12	21
Body-based Reynolds Number, Re_b (10 ³)	23	44	65	217
Advance Ratio, J	0.75	1.02	0.94	1.84
Strouhal Number, <i>St</i>	0.58	0.41	0.45	0.23

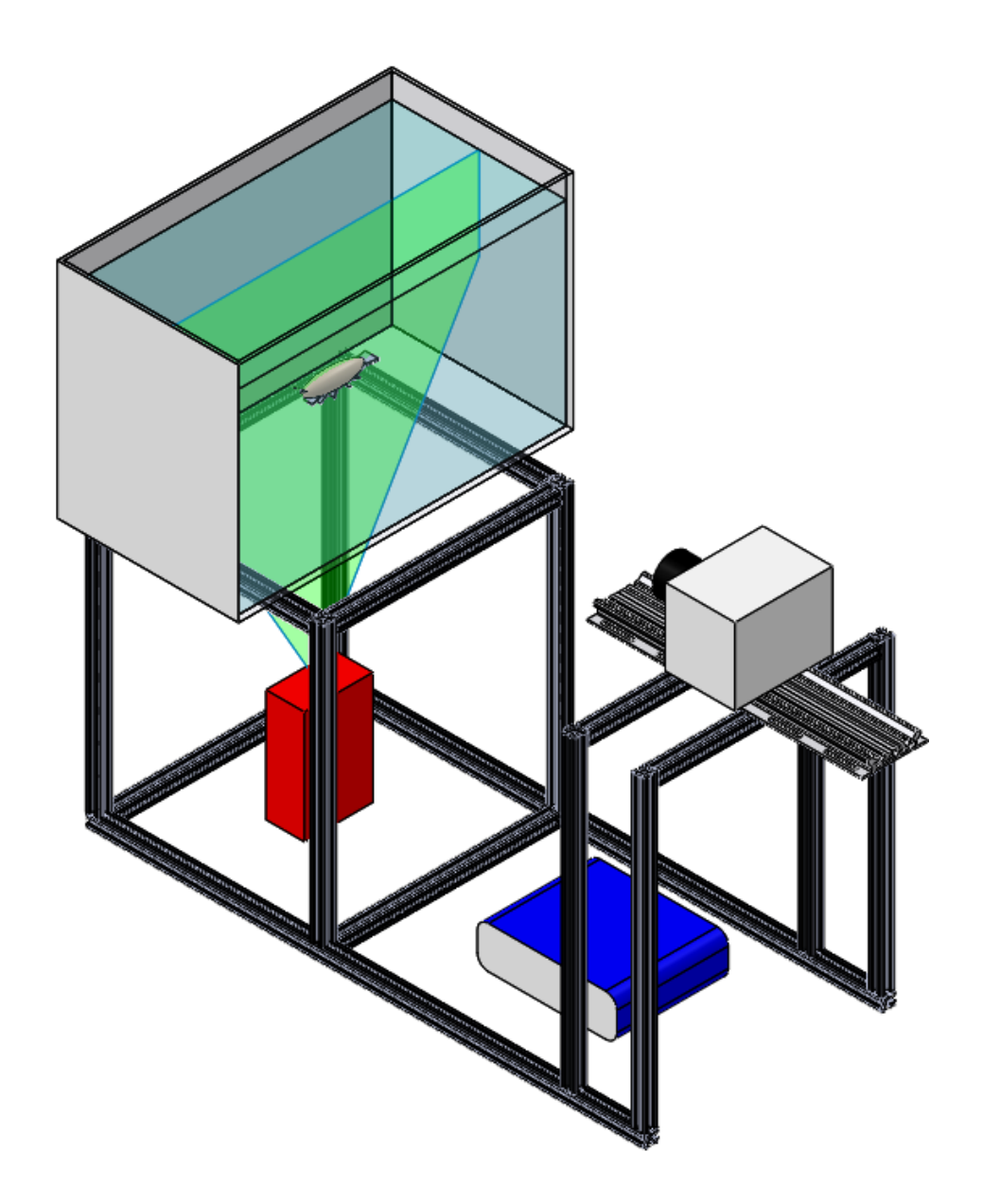


Figure 1. A three-dimensional diagram of the experimental setup showing the laser (red), laser light sheet (green), programmable timing unit (blue), and camera (gray). A model of the mantis shrimp swimming in the light sheet is shown in gray.

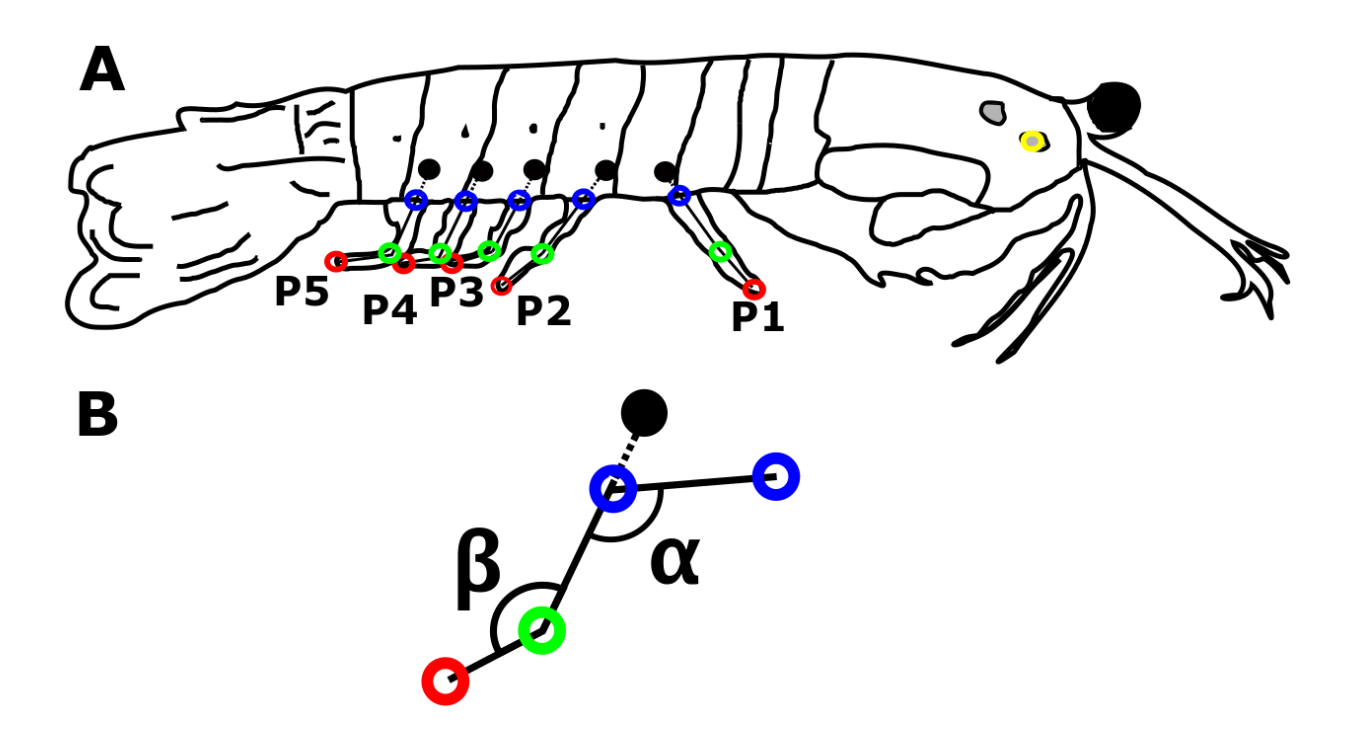


Figure 2. (A) Line drawing of the mantis shrimp and tracked points shown with hollow circles. Pleopods (or pleopod pairs) are named P1 through P5 starting with the anteriormost pleopod. Tip, joint, and base points correspond to red, green, and blue hollow circles, respectively. The articulations of the protopodites with the abdomen are shown with filled black dots. The yellow circle on the carapace was tracked to calculate the swimming speed of the animal. (B) Schematic showing the definition of the stroke angles α and β , with the color coded circles corresponding to the tip, joint, and base points.

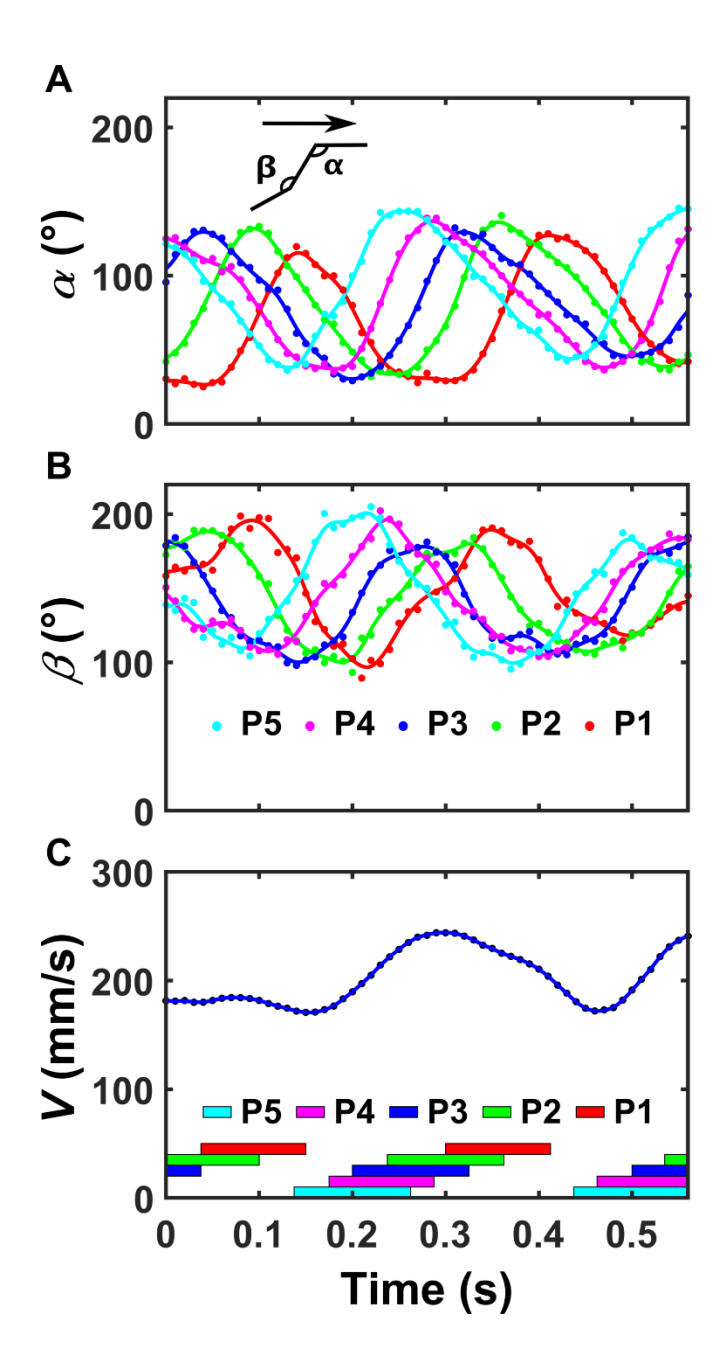


Figure 3. (A) Time history of pleopod angle α for pleopods P1-P5 in Video Sequence 1, in which the mantis shrimp swims at $\bar{V} = 0.20$ m s⁻¹ and f = 3.6 s⁻¹. (B) Time history of pleopod angle β for pleopods P1-P5 in Video Sequence 1. (C) Time history of swimming speed V for Video Sequence 1. Definitions of the angles is shown on diagram in (A) with animal orientation shown with an arrow.

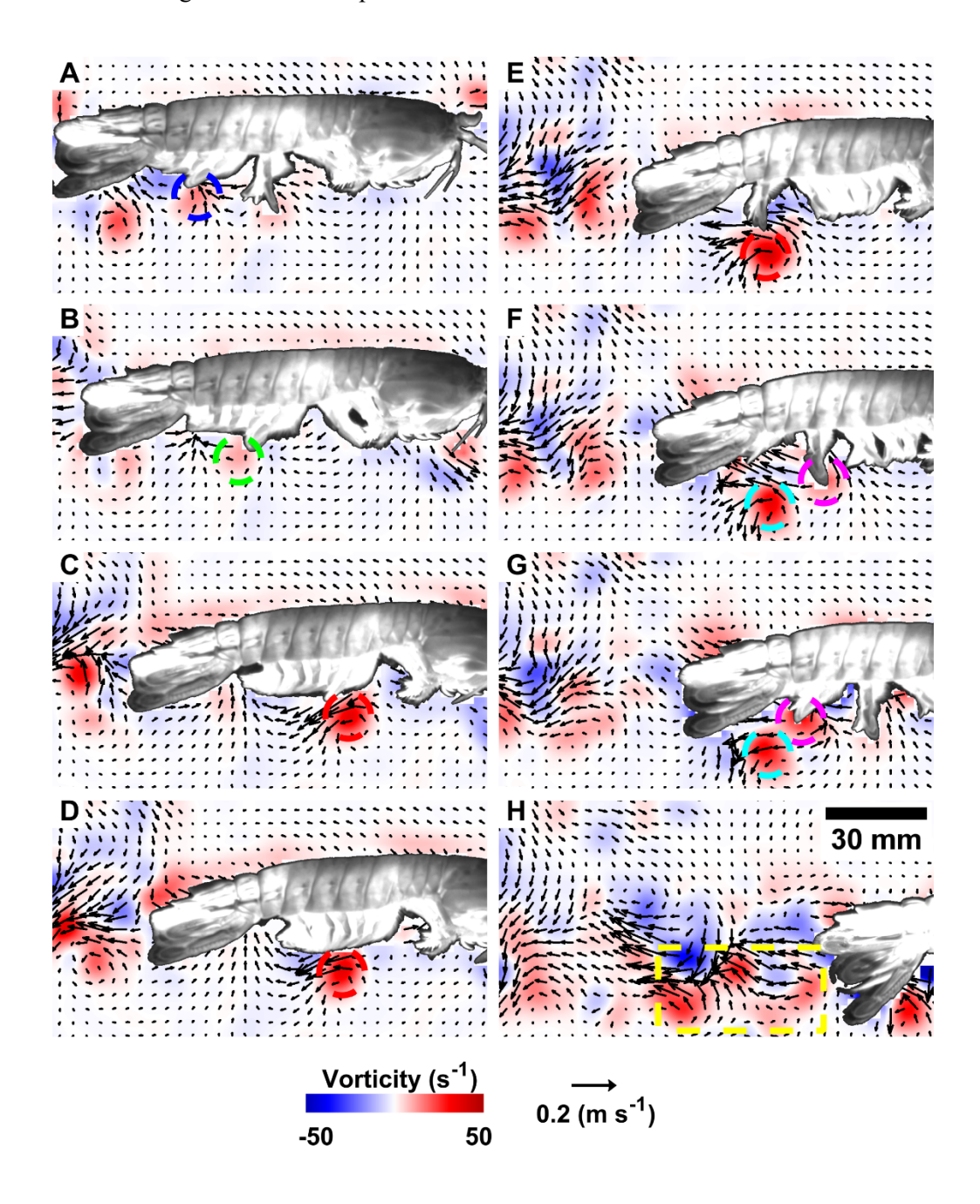


Figure 4. Series of flow fields from Video Sequence 1 showing interpleopod vortex phase matching in which the vortex generated by pleopod pair 1 (P1), indicated by the dashed red circle, is intercepted by pleopod pair 5 (P5). Panels (A), (B), (C), (D), (E), (F), and (G) correspond to time points t=0.315 s, 0.350 s, 0.410 s, 0.440 s, 0.500 s, 0.530 s, and 0.565 s in Fig. 3C. Panel (H), at a later time of t=0.760 s, shows the animal's wake outlined in a dashed yellow box. Dashed circles indicate vortices produced by various

pleopod pairs, with circle color corresponding to pleopod pair as in Figure 3. Vectors represent flow direction and color contours represent vorticity. Vector resolution is 3.9 x 3.9 mm².

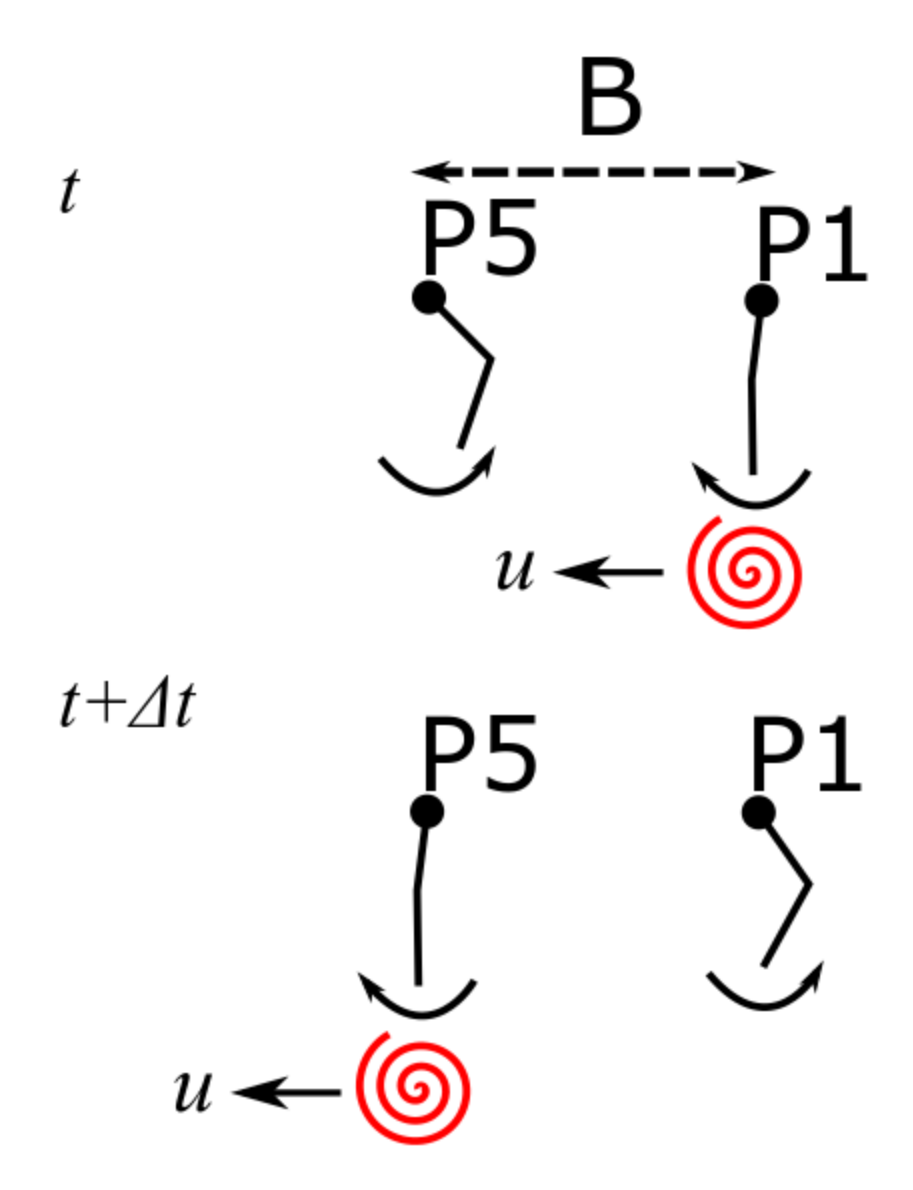


Figure 5. Diagram of the interpleopod vortex phase matching mechanism occurring in metachronal rowing by the mantis shrimp. The vortex (red spiral) created by the power stroke of P1 at time t is shed downstream at a speed u relative to the animal and is intercepted by P5, stroking with a phase lag of Ψ_{P1-P5} , at time $t+\Delta t$, where $\Delta t = B/u$. B is the distance between the base articulations of P1 and P5.